EurJIC
European Journal of Inorganic Chemistry

Full Papers
doi.org/10.1002/ejic.202100711

Chemistry Europe
European Chemical Societies Publishing

Very Important Paper

A Mechanistic Study on the Reaction of Non-Heme Diiron (III)-Peroxido Complexes with Benzoyl Chloride

Markus Lerch,[a] Andreas J. Achazi,[b] Doreen Mollenhauer,[b] Jonathan Becker,[a] and Siegfried Schindler*[a]

Dinuclear iron peroxido complexes are important intermediates for selective oxidation reactions. A detailed kinetic study of the reaction of benzoyl chloride (BzCl) with a dinuclear iron non-heme *cis end-on* peroxido complex with the ligand EtHPTB (*N*,*N*,*N*′,*N*′-tetrakis[(*N*-ethyl-2-benzimidazolyl)methyl]-2-hydroxy-1,3-diamino-propane) had been performed. The starting complex, the iron peroxido complex, can be obtained either by reaction of the iron(II) complex with O_2 or instead, applying the corresponding iron(III) complex together with hydrogen peroxide. Using low temperature stopped-flow measurements allowed to obtain activation parameters and in combination with a Hammet plot it was possible to postulate a mechanism for the formation of a perbenzoate complex prior to its decomposition. Furthermore, the direct reaction of the dinuclear iron(III) EtHPTB complex with peracetic acid was analyzed. Additionally, in comparison a mononuclear non-heme iron complex with the ligand bztpen (*N*-benzyl-*N*,*N*′,*N*′-tris(2-pyridylmethyl)ethane-1,2-diamine) was investigated as well.

Introduction

Selective oxidation/oxygenation reactions of organic substrates are important in the lab and in industry.[1] Efforts to substitute oxidants that are either expensive and/or quite toxic, e.g. chromium(VI) compounds, led to an intensive research on the development of functional model complexes for the active sites of metalloenzymes, especially oxygenases.[2] For example cyanobacterial aldehyde deformylating oxygenase (ADO) catalyzes the conversion of fatty aldehydes into alkanes and formate.[3] Recently Kaizer and co-workers reported the complex $[Fe^{III}_2(\mu\text{-}O_2)(MeBzim\text{-}Py)_4(MeCN)_2]^{4+}$ as a functional model for this enzyme by applying an iron complex with the ligand MeBzim-Py (2-(2′-pyridyl)-*N*-methylbenzimidazole; Scheme 1). In that context they furthermore pointed out the mechanistic versatility of peroxido-diiron(III) intermediates.[4]

We and others have been investigating in great detail the reactivity of iron complexes with the ligand RHPTB (Scheme 1) towards dioxygen and hydrogen peroxide.[5] The dinuclear iron (II) complex $[Fe_2(EtHPTB)(OBz)]^{2+}$ (**1a**, R=Et; EtHPTB = *N*,*N*,*N*′,*N*′-tetrakis[(*N*-ethyl-2-benzimidazolyl)methyl]-2-hydroxy-1,3-diamino-propane) reacts with O_2 to the *cis end-on* peroxido complex $[Fe_2(EtHPTB)(\mu\text{-}1,2\text{-}O_2)(OBz)(X)]^{n+}$ (**2a**, X = solvent or co-ligand).[5c] While under these conditions the formed peroxido complex is only persistent for a short time, it is possible to increase its stability by preparing it from the corresponding iron (III) complexes, $[Fe_2(RHPTB)(X)_m]^{n+}$ in combination with hydrogen peroxide.[5b] This reaction was investigated in acetonitrile as well as in methanol leading to the same results.[6] Furthermore, the reaction of the mononuclear iron(III) complex $[Fe(bztpen)(OMe)](ClO_4)_2$ (**3**$(ClO_4)_2$; bztpen = *N*-benzyl-*N*,*N*′,*N*′-tris(2-pyridylmethyl)ethane-1,2-diamine) with hydrogen peroxide had been analyzed.[7] An *end-on* hydroperoxido complex was formed that could be transformed into a *side-on* peroxido species after the addition of a base.[7b] Interestingly, the corresponding iron (II) complex did not react with dioxygen (neither with carbon monoxide), only with nitrogen oxide a reaction occurred.[7c]

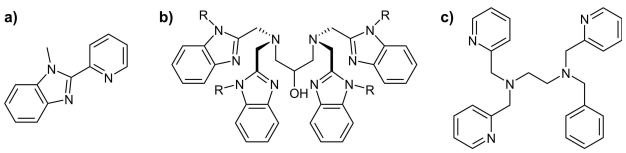

Scheme 1. a) MeBzim-Py, b) RHPTB (R = Et: EtHPTB), c) bztpen.

With regard to the formation of percarboxylate species as important intermediates in oxygenation reactions we report herein our results on the reaction of the iron(III) peroxido complex with EtHPTB as ligand and benzoyl chloride (BzCl) together with some related reactions.

Results and Discussion

The iron(III) complex $[Fe_2(EtHPTB)(OH)_2(MeOH)_2](ClO_4)_3$ (**1b**-$(ClO_4)_3$) was prepared in good yields by reacting the ligand

[a] *M. Lerch, Dr. J. Becker, Prof. Dr. S. Schindler*
Institute of Inorganic and Analytical Chemistry,
Justus-Liebig-Universität Gießen
Heinrich-Buff-Ring 17, 35392 Gießen, Germany
E-mail: siegfried.schindler@anorg.chemie.uni-giessen.de
https://www.uni-giessen.de/fbz/fb08/Inst/iaac/schindler
[b] *Dr. A. J. Achazi, Prof. Dr. D. Mollenhauer*
Institute of Physical Chemistry,
Justus-Liebig-Universität Gießen
Heinrich-Buff-Ring 17, 35392 Gießen, Germany

Supporting information for this article is available on the WWW under https://doi.org/10.1002/ejic.202100711

EtHPTB with iron(III) perchlorate and Et_3N in methanol. The molecular structure of **1 b** is shown in Figure 1 (crystallographic data of **1 b**$(ClO_4)_3$ are reported in the Supporting Information; Figure S2). The molecular structure of this complex is very similar to the complex $[Fe_2(EtHPTB)(H_2O)_2(OMe)(MeOH)](ClO_4)_4$ that had been reported previously by Avenier *et al.*[8] Here, water molecules are coordinated instead of hydroxide anions and one of the methanol ligands is deprotonated. A direct comparison of the two structures reveals that the angle spanned between the iron centers and the alcoholate oxygen is somewhat larger (angle Fe1-O1-Fe2: Avenier 131.1°; this work 128.5°) and this also results in a greater distance between the iron centers (distance Fe1–Fe2: Avenier 3.65 Å; this work 3.61 Å). In contrast to our synthetic protocol described herein, the authors did not apply triethylamine to prepare the iron(III) complex and did not recrystallize the product. Furthermore, **1 b** can be compared with $[Fe_2(HPTB)(\mu\text{-}OH)(NO_3)_2](NO_3)_2$ that had been investigated previously.[9]

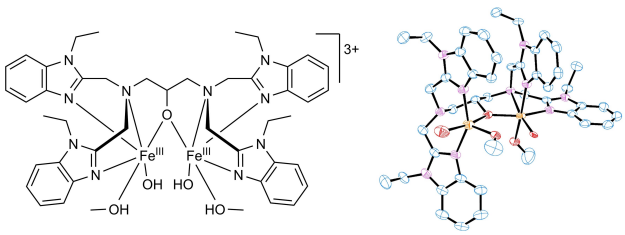

Figure 1. Complex **1 b** $[Fe_2(EtHPTB)(OH)_2(MeOH)_2]^{3+}$ (left). Molecular structure (ORTEP drawing; 50% probability) of the cation of **1 b**$(ClO_4)_3 \times 3$ MeOH. Uncoordinated 3 perchlorate anions and 3 methanol molecules are omitted for clarity (right).

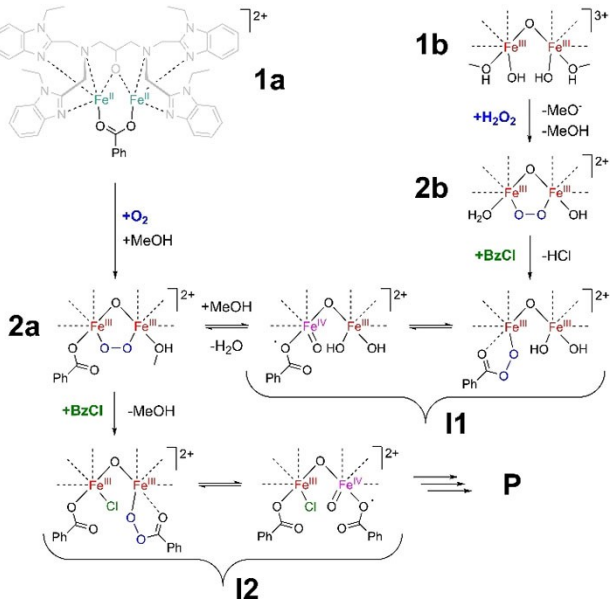

Scheme 2. Proposed reaction mechanism for the formation of **I2**.

Reaction of 1 b with H_2O_2

When a solution of **1 b**$(ClO_4)_3$ was reacted with hydrogen peroxide in methanol, a color change from a pale yellow color to a turquoise color was observed, which indicates the formation of an iron peroxido complex (**2 b**, Scheme 2) as described previously (Figure 2).[5b]

ESI-MS measurements support the assumption that the formation of the peroxido complex $\{[Fe_2(EtHPTB)(\mu\text{-}1,2\text{-}O_2)(OH)(H_2O)] + MeOH\}^{2+}$ is the main species under these conditions (compare Figure S5 and S6). One equivalent of H_2O_2 is enough for complete formation of **2 b** (Figure S9). The reaction in methanol is quite fast (completed within 1 s at RT) and the turquoise-colored solution is stable for a few minutes under these conditions. As previously described, this reaction can be followed by applying stopped-flow techniques.[5b] Time-resolved spectra are shown in Figure 3.

The peroxido complex is characterized by the main absorbance at 605 nm with a molar attenuation coefficient ε of 2200 $L\,mol^{-1}\,cm^{-1}$ under our conditions which compares well with data of the literature with other solvents.[5b,c]

Absorbance vs. time traces under pseudo-first-order conditions ($[H_2O_2] \gg [1\,b]$) could be fitted using single exponential functions. As observed previously a plot of the obtained rate constants k_{obs} vs. the hydrogen peroxide concentration at different temperatures exhibited a linear dependence without

Figure 2. Reaction of **1 b** with hydrogen peroxide, followed by the addition of benzoyl chloride.

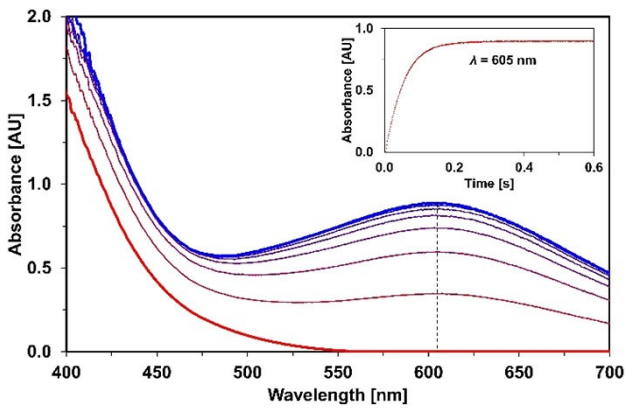

Figure 3. Time-resolved UV-vis spectra ($\Delta t = 0.03$ s) of the reaction between complex **1 b** ($c = 0.4$ mmol L^{-1}) and hydrogen peroxide ($c = 20.0$ mmol L^{-1}) at 25.0 °C in methanol (concentrations after mixing). The inset shows the time-trace of the reaction.

an intercept (Figure 4) and thus leading to an overall second-order rate law (Equation 1).

$$\frac{d[\mathbf{2b}]}{dt} = k_2\,[\mathbf{1b}]\,[H_2O_2] \quad (1)$$

An Eyring plot of the derived second-order rate constants over a much larger temperature range from −50.0 to +25.0 °C (Figure 5) allowed the calculation of the activation parameters to $\Delta H^{\ddagger} = 46 \pm 1$ kJ mol^{-1} and $\Delta S^{\ddagger} = -40 \pm 2$ J mol^{-1} K^{-1}. Data compare reasonable well with previous results of the $[Fe_2(HPTB)(\mu\text{-}OH)(NO_3)_2](NO_3)_2$ with $\triangle H^{\ddagger} = 53 \pm 3$ kJ mol^{-1} and $\triangle S^{\ddagger} = -17 \pm 1$ J mol^{-1} K^{-1} (see Table 1).[5b]

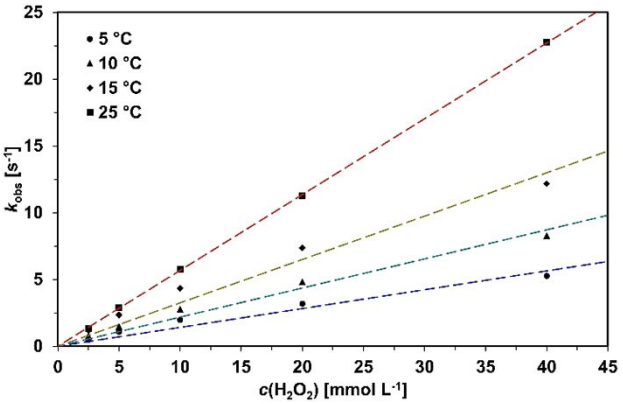

Figure 4. Plot of the rate constants k_{obs} versus H_2O_2 concentration at different temperatures. Complex concentration: $c = 0.2$ mmol L^{-1}. Second-order rate constant $k_{2(25°C)} = 568 \pm 2$ L mol^{-1} s^{-1}.

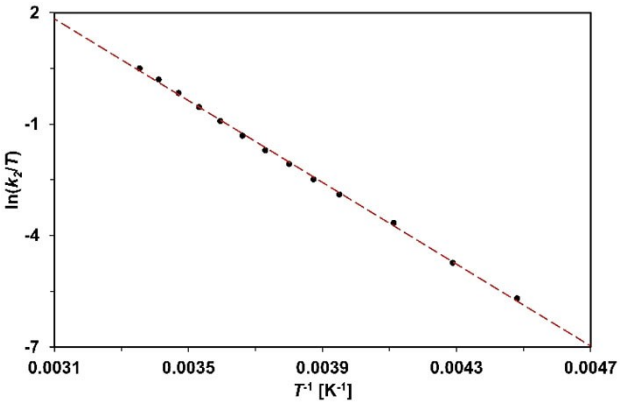

Figure 5. Eyring plot for the reaction of complex **1b** ($c = 0.4$ mmol L^{-1}) with H_2O_2 ($c = 20$ mmol L^{-}1) in the temperature range from −50.0 to 25.0 °C.

Table 1. Summary of molar attenuation coefficient, rate constants and activation parameters of the kinetically investigated reactions in this study.

Reaction in MeOH	BzCl derivative	λ_{max} [nm]	$k_{2\,(25\,°C)}$ [L mol^{-1} s^{-1}]	$\Delta H^{\ddagger}$ [kJ mol^{-1}]	$\Delta S^{\ddagger}$ [J K^{-1} mol^{-1}]
1b + H_2O_2 (→ **2b**)		600	568 ±2	46 ±1	-40 ±2
2b + BzCl (→ **I2**)	BzCl	445	ND	40 ±1	11 ±3
	BzCl	600	9.7 (±0.3) 10^5 [a]	40 ±1	10 ±3
	p NO_2-BzCl	445	ND	67 ±3	21 ±8
	p $N(Me)_2$-BzCl	445	ND	69 ±1	39 ±2
2a + BzCl (→ **I2**)	BzCl	450	243 ±10 [b]	36 ±1	-33 ±6
1b + PAA		440	455 ±25 [c]	32 ±1	-48 ±6

[a] k_3 third-order constant. ND = not determined. [b] At −60 °C. [c] At −65 °C.

Reaction of 2 b with benzoyl chloride

The reaction of the peroxido complex **2b** with BzCl was investigated in methanol because no reaction was observed in acetonitrile (only decomposition of **2b** was detected). Furthermore, we did not assert an influence of different R-groups in RHPTB (Scheme 1) on the reactivity. Iron(III) complexes with the unsubstituted ligand HPTB (R=H) and BnHPTB (R=Bn) showed the same reactivity towards H_2O_2 and the subsequent reaction with benzoyl chloride. As shown in Figure 2 a rapid color change to a gold-brown-colored solution was observed when **2b** was reacted with benzoyl chloride in excess. Time-resolved UV-vis-spectra were recorded in stopped-flow measurements at low temperatures (Figure 6).

The decay of the absorbance maximum at 605 nm of **2b** (premixed immediately prior to the measurement applying an excess of H_2O_2) can be observed while at the same time a new compound is formed, characterized with an absorbance maximum at 445 nm. Two isosbestic points are observed at 415 and 515 nm. Absorbance vs. time traces again could be fitted perfectly well to a single exponential function, however a plot of k_{obs} vs. c(BzCl) turned out to be nonlinear. Instead, to obtain a linear correlation, it was necessary to plot k_{obs} vs. $c(\text{BzCl})^2$ (Figure 7) leading to a third-order rate law with $k_{obs} = k_3\,c(\text{BzCl})^2$ (Equation 2).

$$\frac{d[\mathbf{I2}]}{dt} = k_3\,[\mathbf{2b}]\,[\text{BzCl}]^2 \quad (2)$$

Third-order rate constants obtained here ($k_{3(25°C)} = 9.7 \pm 0.3 \times 10^5$ L^2 s^{-1} mol^{-2}) compare well with those measured for other

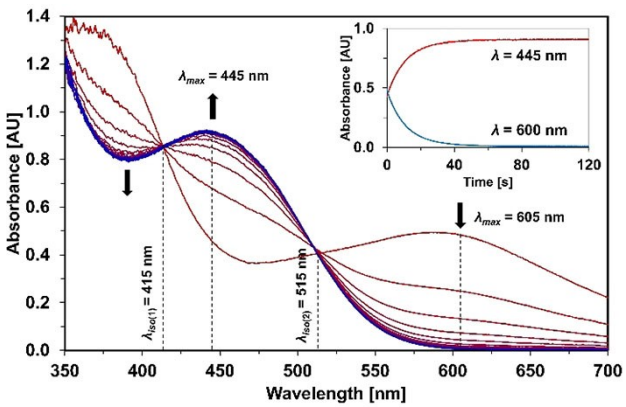

Figure 6. Time-resolved UV-vis spectra ($\Delta t = 7.4$ s) of the reaction between **2b** ($c = 0.2$ mmol L^{-1}, obtained by premixing **1b** with an excess of H_2O_2) and BzCl ($c = 20.0$ mmol L^{-1}) at −80.0 °C. Molar attenuation coefficient $\varepsilon_{445} = 4300$ L mol^{-1} cm^{-1}. The inset shows the time-traces of the reaction.

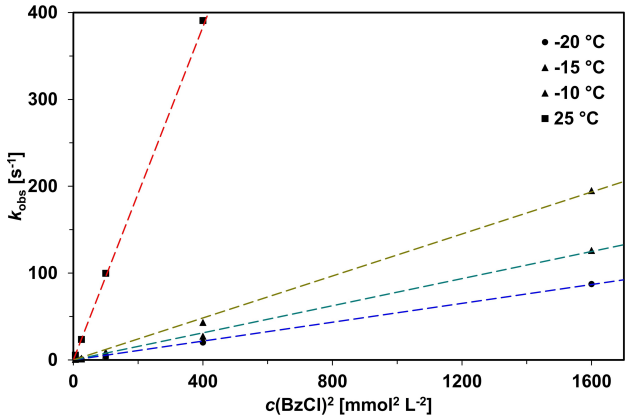

Figure 7. Plot of k_{obs} vs. c(BzCl)^2 at different temperatures. Concentration c(**2b**) = 0.2 mmol L^{-1}.

reactions that showed a third-order rate law e.g. NO + O_2 with a rate constant of 2.1×10^6 L^2 s^{-1} mol^{-2} at 25 °C[10] (depending on the conditions slightly different values)[11] in aqueous solutions and non-aqueous media were obtained.[12]

Since the sole kinetic interpretation does not yet provide any evidence that exactly two benzoyl chloride molecules react with the peroxido complex, a substoichiometric addition was also carried out here. A clear linearity can be seen up to the second equivalent benzoyl chloride added (Figure S10). This observation supports the assumption that exactly two molecules of benzoyl chloride react with **2b** during the reaction with benzoyl chloride. Furthermore, to exclude that benzoyl peroxide is an active reagent herein (it is synthesized in industry from benzoyl chloride with hydrogen peroxide in alkaline solutions), several test reactions with ABTS (2,2′-azino-bis(3-ethylbenzothiazoline-6-sulfonic acid) diammonium salt) were performed. ABTS is a reagent that is used to detect radicals and selectively peroxycarboxylic acids in the presence of H_2O_2.[13] Benzoyl peroxide reacts rapidly with ABTS, however, much slower in comparison with the reaction of complex **2b** with BzCl and hydrogen peroxide. BzCl together with hydrogen peroxide in methanol with a small amount of NaOH only reacts quite slowly with ABTS. Benzoyl peroxide itself does not react with complex **2b**. These experiments clearly indicate that the reaction occurs with BzCl.

From these results we propose that an intermediate, **I1**, is formed from **2b** and BzCl. The Intermediate **I1** stands in a rapid equilibrium with the peroxido complex **2a** which then reacts in a much slower reaction (rate-determining step, RDS) to the metastable product **I2** according to Scheme 2. Other third-order reactions in solution have been described previously (e.g.)[14] with a similar mechanistic scenario. After the very fast formation of **I2**, much slower decomposition reactions took place including the formation of products **P** such as benzoic acid, methyl benzoate, benzoic acid anhydride as well as iron(III) chloride (detected as $[FeCl_4]^-$). These products could be identified by ESI-MS measurements. An ESI-MS measurement of a dilute mixture of **2b** with BzCl in a ratio of 1:2 (measurement performed instantly after mixing) showed the possible formation of $[Fe_2(EtHPTB)(OOBz)(OH)_2]^{2+}$ with m/z = 502.1 as a direct derivative of **I1** (Figure S7). The formation of methyl benzoate and benzoic acid anhydride could be a hint of a free radical mechanism (iron(IV)oxido/benzoato radical-pathway), as these products are formed due to recombination reactions.

For a more detailed analysis we applied *para*-substituted BzCl derivatives with the electron-withdrawing groups –Cl, –NO_2 and electron-donating groups –N(Me)$_2$, –OMe, –Me for the reaction with **2b**. Besides BzCl (temperature range between −80.0 and 0.0 °C) we performed measurements with *p*N(Me)$_2$-BzCl and *p*NO_2-BzCl in a temperature range between 15.0 and 50.0 °C. From the temperature dependence the corresponding Eyring plots (Figure S11) allowed calculations of the activation parameters with BzCl: $\Delta H^{\neq} = 40\pm1$ kJ mol^{-1} and $\Delta S^{\neq} = 10\pm3$ J mol^{-1} K^{-1}; *p*N(Me)$_2$-BzCl: $\Delta H^{\neq} = 69\pm1$ kJ mol^{-1}, $\Delta S^{\neq} = 39\pm2$ J mol^{-1} K^{-1}; *p*NO_2-BzCl: $\Delta H^{\neq} = 67\pm3$ kJ mol^{-1}, $\Delta S^{\neq} = 21\pm8$ J mol^{-1} K^{-1} (see Table 1). The slightly positive activation entropies indicate a dissociative interchange mechanism.

Hammett Plot

The Hammett correlation (a linear free energy relationship) is a widely used method to evaluate the impact of electrosterical effects on reactions. This correlation allows conclusions to be drawn about the transition state of the rate-determining step (RDS) of the observed reaction. Figure 8 shows the Hammett plot for the reaction of **2b** with *para*-substituted benzoyl chloride. In this study only *para*-substituted benzoyl chlorides were used, due to possible steric hindrance of *meta*-substituents. The Hammett plot leads to a V-shape from the two linearly fitted points that intersect near by a σ-value of 0 (unsubstituted BzCl).

Overall it is obvious, that electron-withdrawing (*p*Cl, *p*NO_2) and electron-donating (*p*N(Me)$_2$, *p*OMe, *p*Me) substituents slowed down the reaction. The V-shape indicates a change in the reaction mechanism, in which the electron-rich *p*N(Me)$_2$-BzCl is more nucleophilic ($\rho = -1.996$) and the electron-poor *p*NO_2-BzCl is more electrophilic ($\rho = 0.477$). This provides

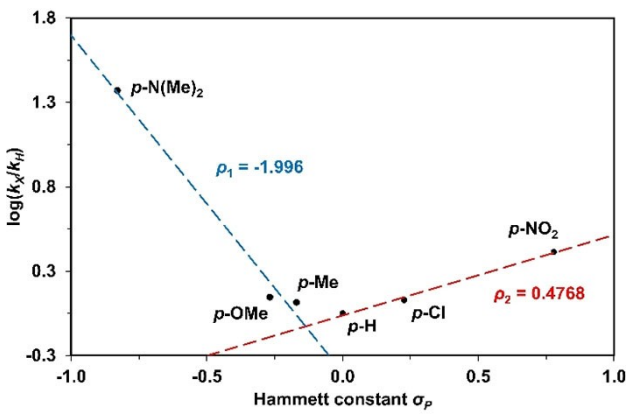

Figure 8. Hammett plot for the reactions of **2b** with *para*-substituted BzCl-derivatives (substituent = –N(Me)$_2$, –OMe, –Me, –Cl, –NO_2) at −60.0 °C in MeOH.

valuable information about the location of the RDS and transition state (TS). The strong negative ρ-value clearly indicates a build-up of a positive charge in the TS of the RDS, whereas the slightly positive ρ-value indicates a build-up of a positive charge in the TS of the RDS. In combination with the slightly positive activation entropies of the reaction between **2b** and pNO$_2$-BzCl resp. pN(Me)$_2$-BzCl (indicating a dissociative interchange mechanism) two different reaction pathways can be proposed. A possible mechanism for both reaction pathways is presented in Scheme 3.

In the reaction pathway with pN(Me)$_2$-BzCl, the C–Cl bond is severely weakened or even broken in the TS of the RDS, which is due to the high positive charge on the carbonyl carbon. On the other hand, the slightly positive ρ-value in the pNO$_2$–BzCl reaction pathway can be interpreted as a partially accomplished nucleophilic attack on the carbonyl carbon of the benzoyl chloride. In any case, it can be confirmed that benzoyl chloride is actively involved in the RDS of the whole reaction sequence.

In contrast to our system, no effect on para-substitution was observed with the system of Kripli and co-workers, where a ρ-value of zero was obtained.[4] Therefore, for their reaction mechanism a nucleophilic attack of the peroxido-diiron(III) complex as rate-determining step had been excluded.

Reaction of iron(II) complex 1a with O_2 and benzoyl chloride

As described in the introduction, the iron(II) complex $[Fe_2(EtHPTB)(OBz)]^{2+}$ (crystallographic data of **1a**$(BPh_4)_2$ are reported in the Supporting Information; see Figure S1) reacts with dioxygen to form the peroxido complex **2a** (Scheme 2). Therefore, to gain further support for the proposed mechanism of the reaction of **2b** with BzCl we also investigated the reaction of **2a** with BzCl (the benchtop experiment is reported in the Supporting Information, Figure S12 and S13). To accomplish this we used a double-mixing stopped-flow unit with four syringes (syringe 1: solution of **1a**; syringe 2: solvent saturated with dioxygen; syringe 3: solvent saturated with argon; syringe 4: solution of BzCl). Because of the poor solubility of **1a**$(BPh_4)_2$ in MeOH, the reaction was performed with 5% MeCN as co-solvent. Time-resolved UV-vis spectra of this reaction are presented in Figure 9.

A plot of the k_{obs}-values vs. BzCl-concentration allowed a linear fit with an intercept C (Figure S13) leading to an overall second-order rate law (Equation 3).

$$\frac{d[\mathbf{I2}]}{dt} = k_2\,[\mathbf{2a}]\,[\mathrm{BzCl}] + C \qquad (3)$$

The reaction is a bit faster than the reaction of **2b** with BzCl. However, this is easy to understand because here a benzoate is already coordinated to the complex and therefore only has to react further with BzCl. Overall, this supports our postulated mechanism (Scheme 2). The reaction was measured in a temperature range between −70.0 and −40.0 °C and from an Eyring plot (Figure S14) of the second-order rate constants the activation parameters could be calculated to $\Delta H^{\ddagger} = 36 \pm 1\ \mathrm{kJ\,mol^{-1}}$ and $\Delta S^{\ddagger} = -33 \pm 6\ \mathrm{J\,mol^{-1}\,K^{-1}}$ (see Table 1). The slightly negative activation entropy indicates an interchange associative mechanism, again in accordance with our postulated mechanism. The intercept we observed for the plot of the k_{obs}-values vs. c(BzCl) (Figure S14) is a bit more difficult to interpret. While we think we can exclude a reversible reaction at this point it could be possible that to some part acetonitrile is coordinated that needs to dissociate prior to the bonding of BzCl, leading to a reaction step independent of c(BzCl) and thus causing an intercept. However, it also could be caused by the equilibrium between **2a** and **I1**.

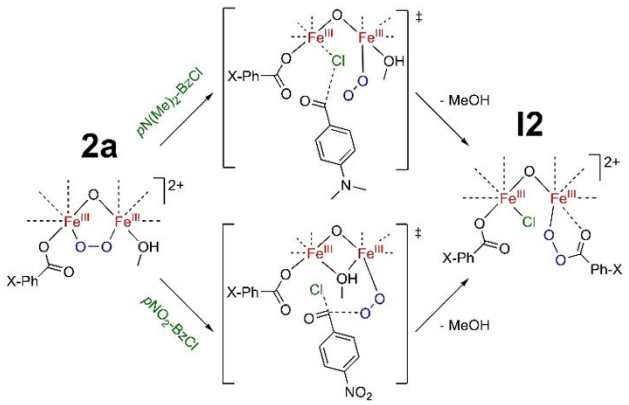

Scheme 3. Postulated mechanisms in dependence on different benzoyl chloride derivatives (electron-withdrawing or electron-donating groups in para position).

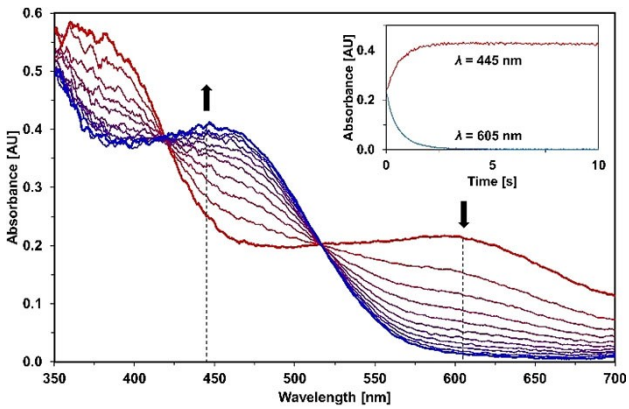

Figure 9. Time-resolved UV-vis spectra ($\Delta t = 0.14$ s) acquired from a double-mixing stopped-flow experiment in MeOH (5% MeCN) as cosolvent. The intermediate **2a** was generated by mixing 75 µL of solution **1a** ($c = 0.4\ \mathrm{mmol\,L^{-1}}$) with 75 µL oxygen-saturated methanol solution ($c = 10.4\ \mathrm{mmol\,L^{-1}}$). The first mixed solution was aged for 3 s. In the second mixing the generated peroxido complex **2a** reacted with 75 µL BzCl solution ($c = 40\ \mathrm{mmol\,L^{-1}}$) at −70 °C to trace the chromophore at $\lambda_{max} = 445$ nm (intermediate **I2**) and the decay of the peroxido complex **2a** at $\lambda_{max} = 605$ nm. The inset shows the time-traces over the course of 10 s.

DFT calculations

To gain further insights into the reaction from **2 b** with benzoyl chloride via the (assumed) **I1**, **2 a** and (assumed) **I2** to give a possible product **P**, a computational analysis was performed. The equilibrium structures and Gibbs energies of the involved complexes in solution were calculated with DFT for the concentrations used in the experiment (see Computational details). The results of the calculations are shown in Scheme 4.

The low-spin state with 0 unpaired electrons (singlet state with total spin quantum number $S=0$), the triplet state ($S=1$), quintet state ($S=2$), the septet state ($S=3$), nonet state ($S=4$) and the high-spin state with 12 unpaired electrons (tridecet state with total spin quantum number $S=6$) were energetically unfavorable for **2 b**, **I1-a**, **2 a** and **I2-a**. Instead, the undecet spin state ($S=5$) is most favorable for these iron complexes. The other iron complexes (Scheme 4) are very similar to **2 b**, **I1-a**, **2 a** and **I2-a**; therefore, we calculated them in an undecet spin state ($S=5$) as well. For the first step we assume that **2 b** reacts to **I1-a** (see Scheme 4). The reactions is exergonic and a Gibbs energy of $-48.1\ kJ\,mol^{-1}$ is gained. Three additional isomers (**I1-b** to **I1-d**) have been calculated for this step, but all are energetically less favorable. **I1-a** and **I1-c** are in agreement with the structures proposed in Scheme 2. The benzoate radical in complexes **I1-c** and **I1-d** is only loosely attached to the rest of the complex via π-π interaction and C–H···O hydrogen bonds. Thus, the iron atoms remain Fe^{III}. Furthermore, the spin state of the benzoate radical should have nearly no effect on the rest of the complex due to the large distance or loose attachment. Indeed, the nonet spin state ($S=4$) for **I1-c** and **I1-d** is energetically only $+0.1\ kJ\,mol^{-1}$ higher than the undecet spin state ($S=5$) for the same molecular structure.

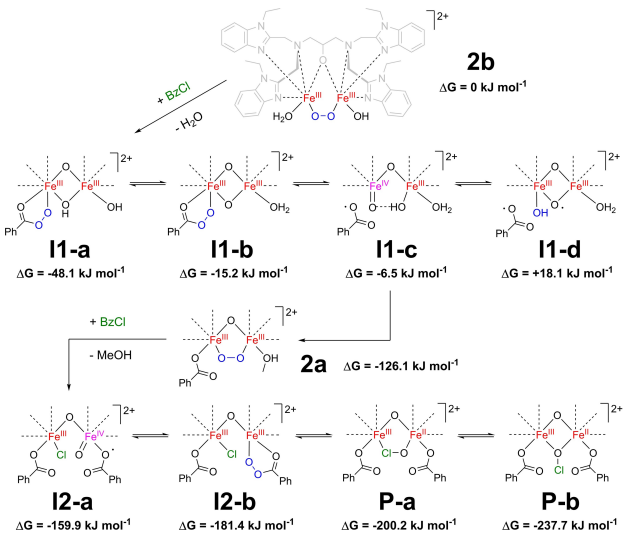

Scheme 4. Gibbs energies relative to **2 b** in conjugation with BzCl. c(BzCl) = 0.04 mol L^{-1}. The electronic energies are calculated with B3LYP*-D3(BJ)/def2-TZVP COSMO(methanol). The ro-vibrational contributions are calculated with PBE0-D3(BJ)/def2-SVP, def2-TZVP. All iron complexes are in an undecet spin state ($S=5$).

Next an intramolecular formation takes place in **I1-a**, water is released, methanol binds to one iron atom resulting in **2 a**. The reaction is exergonic and a Gibbs energy of $-78.0\ kJ\,mol^{-1}$ is gained. From there, we assume that **2 a** reacts to **I2-a** and a Gibbs energy of $-33.8\ kJ\,mol^{-1}$ is gained. The shortest bond distance between an oxygen atom of the benzoate radical and the Fe^{IV}=O group of the undecet **I2-a** is 2.99 Å. This is a very long, and therefore, a weak bond. For comparison the bond distance between the benzoate anion and the Fe–Cl group of the undecet **I2-a** is only 1.96 Å. Like for **I1-c** and **I1-d**, the spin state of the loosely attached benzoate radical has nearly no effect on the rest of the **I2-a** complex. Hence, the nonet spin state is energetically very close to the undecet spin state (only $+0.5\ kJ\,mol^{-1}$ higher for the same molecular structure). As shown in Scheme 4, the benzoate radical in **I2-a** can react to a peroxybenzoate (**I2-b**). This intramolecular reaction is exergonic by $-21.5\ kJ\,mol^{-1}$ and both, the third oxygen of the peroxybenzoate and the chloride form weak bonds to the iron, which is connected to the peroxybenzoate. These results are in agreement with the proposed reaction in Scheme 2.

A possible next step is the intramolecular formation of a hypochlorite (**P-a**). The hypochlorite can reorient itself forming **P-b**, which is the most stable complex found in this study. The reaction from **2 a** over **I2-a**, **I2-b**, and **P-a** up to **P-b** is thermodynamically favorable. The formations of **I2-a**, **I2-b**, and **P-a** involve either the breaking or formation of an oxygen-oxygen bond as a key step. Thus, possible reaction barriers can be expected to be similar in all these cases.

Reactions of 1 b with peracids

To gain a better understanding of the overall mechanistic scenario **1 b** was furthermore reacted with percarboxylic acids. We excluded perbenzoic acid due to the danger involved with this compound and chose peracetic acid (PAA), *m*-chloroperbenzoic acid (mCPBA) and perdecanoic acid (PDA) instead. Perdecanoic acid was prepared according to the synthesis reported by Sitko *et al.*, however, so far no crystal structure of this compound had been reported.[15] We obtained crystals of perdecanic acid and the molecular structure together with crystallographic data are presented in the Supporting Information (Figure S4 and Table S4).

When **1 b** was reacted with an excess PAA in methanol, an orange-brown-colored solution formed (Figure S15) and peracetic acid adduct compounds could be detected in an ESI-MS spectrum (Figure S8). A *m/z* ratio at 1123.1 shows the presence of the peracetato complex $[Fe_2(EtHPTB)(OOAc)(OH)](+2ClO_4)^+$. In Figure 10 the characteristic UV-vis bands of the intermediates (**1 a** + O_2 + BzCl, **1 b** + H_2O_2 + BzCl and **1 b** + PAA) are compared.

Comparison with data from the literature for UV-vis data for iron(III) peroxyacetate complexes (in acetonitrile) are in accordance with our data and therefore also support our assignment of a peroxybenzoate complex discussed above.[16]

Efforts to crystallize and structurally characterize the intermediates **I1/I2** have been unsuccessful. So far (to the best of our knowledge) only one example of a structurally character-

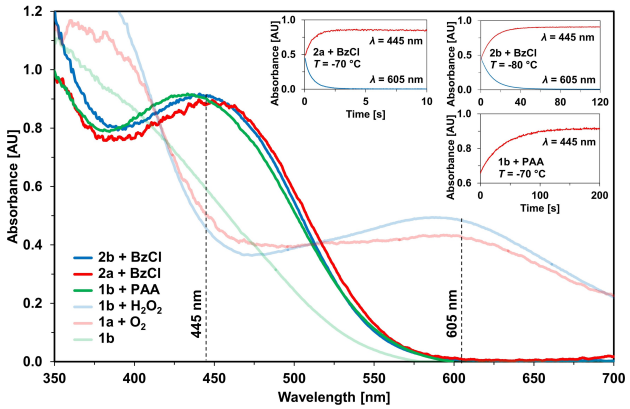

Figure 10. Comparison of the UV-vis spectra. The spectra of the monitored reactions were used, which showed the maximum absorption at 445 nm and 605 nm.

ized mononuclear non-heme iron(III) complex with a coordinating percarboxylic acid (PAA) had been reported.[17] However its UV-vis spectrum is completely different to the other known peroxyacetate iron complexes.

Time-resolved UV-vis spectra of the reaction of **1 b** with an excess of PAA (formation of **I2'**) at low temperatures are reported in the Supporting Information (Figure S15). A plot of k_{obs} values vs. *c*(PAA) could be fitted linear through the origin (Figure S16) leading to a second-order rate law (Equation 4).

$$\frac{d[\mathbf{I2'}]}{dt} = k_2\,[\mathbf{1b}]\,[PAA] \qquad (4)$$

An Eyring plot at temperatures between −70.0 and −40.0 °C (Figure S17) provides the activation parameters: $\Delta H^{\neq} = 32 \pm 1$ kJ mol^{-1} and $\Delta S^{\neq} = -48 \pm 3$ J mol^{-1} K^{-1} (see Table 1) indicating an interchange associative mechanism.

Reaction of **1 b** with mCPBA was sluggish and was not investigated further. A similar observation was described previously by Furutachi and co-workers.[17] PDA was applied in order to be able to react a highly pure peracid with complex **1 b** and thus to exclude other interfering components such as water. When analyzing time-resolved UV-vis spectra, only the formation of a peroxido adduct could be detected at low concentrations of percarboxylic acids. This is probably due to the direct oxidation of the coordinated hydroxides. However, applying high concentrations of the peracids PAA, mCPBA or PDA the formation of gold-brown-colored product solutions was observed. While the PAA adduct is stable for weeks at low temperatures the solutions of the mCPBA and PDA adducts turned to a blue-green-colored solution at −80 °C in less than an hour. Furthermore, PAA as well as mCPBA were tested for their reaction towards ABTS. The reaction turned out to be quite slow: about 3 min for peracetic acid and approximately 10 min for mCPBA.

Reactions with NEt_3

If the percarboxylate complex formed by the reaction of **2 b** + BzCl was reacted with NEt_3, a peroxido complex formed (the benchtop reaction is shown in Figure S18). Time-resolved spectra of the reaction of NEt_3 with premixed **2 b** + BzCl were obtained again with our double-mixing stopped-flow unit with four syringes and are presented in Figure 11. A plot of k_{obs} vs. [NEt_3] showed a linear dependence with intercepts (Figure S19).

This indicates a parallel or back reaction, most likely based on an acid/base equilibrium under the conditions applied.

An Eyring plot obtained from the k_2 values of the main reaction (Figure S20) did lead to the activation parameter $\Delta H^{\neq} = 49 \pm 1$ kJ mol^{-1}, $\Delta S^{\neq} = 9 \pm 4$ J mol^{-1} K^{-1}. With an activation entropy close to 0 this reaction follows an interchange pathway. The same reaction behavior was observed when premixed **1 a** + PAA (instead of **2 b** + BzCl) was reacted with NEt_3.

Reaction of $[Fe(bztpen)OOH]^{2+}$ with BzCl

To compare our results of a dinuclear iron complex system with a mononuclear iron complex we also investigated the reaction of the iron(III) complex with bztpen as ligand (Scheme 1). The complex [Fe(bztpen)(OMe)]$(ClO_4)_2$ (**3**$(ClO_4)_2$) has been prepared under aerobic conditions in methanol by combining bztpen, $Fe(ClO_4)_3$ and Et_3N in a ratio of 1:1:1. Crystals were obtained and the molecular structure together with crystallographic data are reported in the Supporting Information (Figure S3 and Table S3). The molecular structure compares well with [Fe^{III}-(bztpen)(OMe)]$(PF_6)_2$ reported previously.[18] It is well known from previous work that this complex reacts with hydrogen peroxide to a purple-colored *end-on* hydroperoxido complex, $[Fe(bztpen)(OOH)]^{2+}$.[7b] Time-resolved UV-vis spectra of this reaction are reported in the Supporting Information (Figure S21)

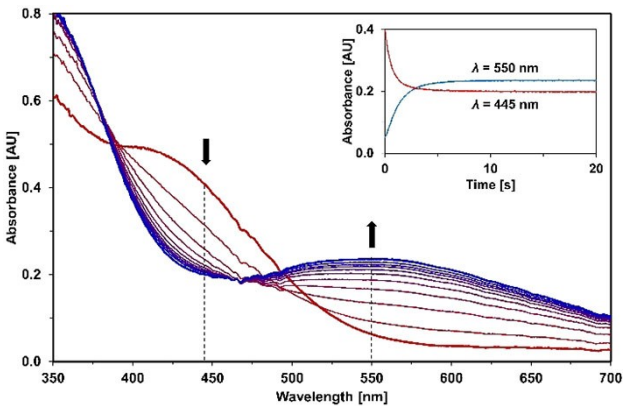

Figure 11. Time-resolved UV-vis spectra (Δ*t* = 0.42 s) acquired from a double-mixing stopped-flow experiment in MeOH. The intermediate **I2** was generated by mixing 75 μL of a premixed solution of **2 b** (*c* = 0.4 mmol L^{-1}) with 75 μL H_2O_2 solution (*c* = 20 mmol L^{-1}). The first mixed solution was aged for 5 s. In the second mixing the generated intermediate **I2** reacted with 75 μL of an Et_3N solution (*c* = 80 mmol L^{-1}) at 0 °C to trace the decay at λ = 445 nm (**I2**) and the formation of a peroxido complex at λ_{max} = 550 nm. The diagram in the right corner shows the time-trace over the course of 20 s.

and kinetic data fit well with our previous results. However, in contrast to the reaction of **2b** with BzCl the reaction of $[Fe(bztpen)(OOH)]^{2+}$ with BzCl is complex (time resolved UV-vis spectra of this reaction are reported in the Supporting Information, Figure S22), indicating additional reactions take place that so far could not be analyzed.

In a subsequent reaction with a base such as Et_3N the hydroperoxido complex reacts to the corresponding *side-on* peroxido complex (turquoise). Interestingly, while the hydroperoxido complex reacts quite fast with benzoyl chloride the *side-on* peroxido complex did not react at all with BzCl.

Summary and Conclusion

In summary, we have studied the kinetics of the formation of peroxido complex **2b** (Fe^{III} complex **1b** + H_2O_2) and the subsequent reaction with benzoyl chloride in methanol in detail. We assume that the chromophore formed with λ_{max} = 445 nm is an iron(IV)oxido/carboxylato radical species **I1** that alternatively had been described as an iron(V)oxido-/carboxylato species (for PAA systems) according to the following equilibria presented in Scheme 5.[16a–c,e–i,19]

It turned out that the peroxido complex **2a**, formed in the reaction between Fe^{II} complex **1a** and O_2, was also able to react in the same way to form the chromophore at λ_{max} = 445 nm.

In contrast to previous publications that reported formation of iron(III)percarboxylates (mainly peracetate) in acetonitrile, our intermediates **I1/I2** herein were formed in the protic solvent methanol. Detailed kinetic studies were performed for the reaction of the peroxido complexes with benzoyl chloride and furthermore, the reaction of the iron(III) complex **1b** with peracetic acid.

From our kinetic investigations including a Hammet analysis we could propose a mechanism for the formation of the reactive intermediates, which is supported by a thermodynamic consideration of various intermediates using DFT calculations. They showed that the iron(III) species are more stable than the species with higher oxidized iron. The intermediates finally decompose to an almost colorless mixture of products that only in part could be identified.

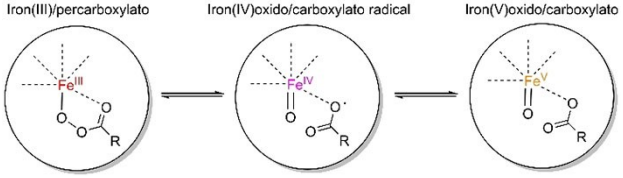

Scheme 5. Illustration of the possible equilibria between iron(III)/percarboxylato-, iron(IV)oxido/carboxylato radical- and iron(V)oxido/carboxylato-species.

Experimental Section

General: All solvents were distilled before use. Extra dry and oxygen-free solvents were distilled using desiccants under an argon atmosphere. Commercially available chemicals were used without further purification. Abbreviations of the supplier: Alfa Aesar (AA), CARL ROTH (CR), J&K Scientific (J&K), PanReac AppliChem ITW Reagents (PRAC), ACROS ORGANIC (AO), Sigma Aldrich (SA), FluoroChem (FC). Methanol extra dry (AO; 99.9%), acetonitrile extra dry (AO; 99.9%), 4-(dimethylamino)benzoyl chloride (J&K, 97%), 4-methoxybenzoyl chloride (J&K, 99%), 4-methylbenzoyl chloride (J&K, 98%), benzoyl chloride (SA; 99%), 4-chlorobenzoyl chloride (J&K, 99%), 4-nitrobenzoyl chloride (SA; 99%), 1,3-diamino-2-propanol-*N,N,N′,N′*-tetraacetic acid (TCI; 98%), 1,2-phenylenediamine (AA; 98%), 2-chloromethyl-pyridine hydrochloride (FC; 97%), *N*-benzylethylenediamine (AA; 98%), trifluoromethanesulphonic acid (abcr; 99%), iron powder (AA; 99%), iron(III) perchlorate nonahydrate (SA; 98%), iron(III)triflate (AA; 90%), benzoic acid (AA; 99%); decanoic acid (TCI; 98.0%), hydrogen peroxide (CR; 50% solution in H_2O), peracetic acid (PRAC; 15% solution in H_2O), urea hydrogen peroxide (SA; 97%), 2,2′-azino-bis(3-ethylbenzothiazoline-6-sulfonic acid) diammonium salt (AA; 98%). Pure iron(II) triflate•diacetonitrile salt was synthesized according to the literature.[20]

Physical Measurements: ^{1}H- and ^{13}C-NMR spectra were recorded on a Bruker Avance II 200 spectrometer (^{1}H at 200 MHz; ^{13}C at 50 MHz), Bruker Avance II 400 spectrometer (^{1}H at 400 MHz; ^{13}C at 100 MHz) and Bruker Avance III HD 400 spectrometer (^{1}H at 400 MHz; ^{13}C at 100 MHz) in deuterated solvents using TMS as internal standard. The ^{1}H- and ^{13}C-NMR spectra were calibrated against the proton and carbon signals of tetramethylsilane.

ESI-MS Measurements: Electrospray-ionization MS (ESI-MS) measurements in MeOH were performed on a Bruker micro-TOF mass spectrometer. When measuring any percarboxylato species, the corresponding solutions were pre-cooled to a temperature just above the melting point of methanol using liquid nitrogen. After mixing of the complex and the reagent, the cooled solution was measured immediately.

Stopped-Flow-Technique: Kinetic studies of the reactions of hydrogen peroxide with iron(III)complexes were recorded on a modified Hi Tech SF-3L low-temperature stopped-flow unit (modification for possible double-mixing measurements; Salisbury, U.K.) equipped with a J&M TIDAS 16-500 diode array spectrophotometer (J&M, Aalen, Germany). The kinetic data were treated by a global analysis fitting routine using the program Kinetic Studio (v.4.0.113798, T_gK Scientific) and/or by extracting single absorbance vs. time traces at different wavelengths. These traces were fitted to single-exponential functions using the integrated J&M software Kinspec. Hydrogen peroxide solutions were prepared by adding hydrogen peroxide (50%, cerimetric titration) with micropipets to the solution. In order to investigate the Intermediates **I1/I2** using the stopped-flow technique, complex **1b** was treated with an excess of H_2O_2. This premixed solution is taken up in the stopped-flow syringes and used as usually. For measurements where moisture and or air/oxygen should be avoided, the stopped-flow syringes were prepared in a glovebox by MBraun under an argon atmosphere. The reaction between **1a** and O_2 and the subsequent reaction with benzoyl chloride was performed with the double-mixing stopped-flow option. Dioxygen concentration in a saturated methanol solution has been reported to be 10.4 mmol L^{-1} at 25 °C.[21]

Computational Details: All structure optimizations were performed with B3LYP*-D3(BJ)/def2-TZVP,[24] the multipole accelerated resolution-of-identity (RI) approximation for *J* (MARI-*J*, with default parameters), Fermi-smearing, the "multiple grid" m4 for the

quadrature of exchange-correlation terms,[24f] and the dielectric continuum solvent model COSMO[25] (simulating methanol, relative permittivity $\varepsilon_r = 32.6$, refractive index $n_D = 1.3288$) using the Turbomole 7.5 software package.[26] Several studies have shown that for iron complexes, B3LYP with 15% HF exchange (called B3LYP*)[24c] is the density functional that comes closest to the experimental data.[24c,27] Furthermore, Kepp[27b] showed that the results for B3LYP* (with 15% HF exchange) can be improved by adding the D3(BJ) dispersion correction of the original B3LYP density functional. The ro-vibrational contributions are calculated for all molecules at the PBE0-D3(BJ)/def2-SVP, def2-TZVP[24,28] level seminumerical with the NumForce script including the fast contribution of the solvent in Turbomole 7.3 software package.[29] The def2-SVP[24f,28d] basis set was used for all atoms except iron. For iron the def2-TZVP[24e] was employed. For MARI-*J* the default parameter from older Turbomole versions were used to speed up calculations: precision: 10^{-6}, lmaxmom: 10, thrmom: 10^{-18}. The frequency calculations also verified the found molecular structures as minima (at the PBE0-D3(BJ)/def2-SVP, def2-TZVP level of theory). At the B3LYP*-D3(BJ)/def2-TZVP level of theory various spin states ($S=0$, $S=1$, $S=2$, $S=3$, $S=4$, $S=5$ and $S=6$) were tested and the undecet spin state was found to be the most stable. The same concentration was used as in the experiment starting from the peroxide complex **2b**: Methanol 24.66 mol L^{-1}, benzoyl chloride 0.04 mol L^{-1}, and all the iron complexes 0.4 mmol L^{-1}. The experiments starting from **2a** were performed with a benzoyl chloride concentration of 20 mmol L^{-1}, the results are given in Scheme 4. The concentration is included via the translational entropy. This results in the following correction term G_{corr} for the Gibbs energy (Equation 5).

$$G_{corr} = -RT\ln\left(\frac{V_m^{new}}{V_m^{old}}\right) \quad (5)$$

with the molar gas constant R, the temperature T and the new (V_m^{new}) and old ($V_m^{old} = 0.024789598\ m^3$) volume of 1 mol of substance.

Synthesis of *N,N,N′,N′*-Tetrakis(2-benzimidazolylmethyl)-2-hydroxo-1,3-di-aminopropane (HPTB): The synthesis was performed according to the procedure by McKee *et al.*[22] 5.00 g diamino-2-propanol-*N,N,N′,N′*-tetraacetic acid (15.5 mmol) and 10.07 g *o*-phenylenediamine (93.09 mmol) were grounded together. The powder was taken up in a 250 mL Schlenk-flask and heated to 180 °C over 1.5 h. After cooling to RT the reddish glass was grounded and dissolved in 250 mL 4 mol L^{-1} HCl. After a few minutes a colorless solid precipitated. The solids were filtered and washed with ice-cold water. The filter residue was dissolved in 250 mL water. The solution was basified by adding 5 mol L^{-1} NaOH solution. After 10 min the colorless solid was filtered and washed a few times with water until the filtrate shows no alkaline reaction. The filter residue was air dried and then dissolved in 200 mL of hot acetone. At room temperature the mixture was mixed with 100 mL H_2O. The precipitation was completed at 4 °C overnight. The solids were filtered and washed with water. The filter residue was first air-dried and then dried in a desiccator over P_2O_5 under vacuum. The product was obtained as voluminous colorless powder (8.615 g, 14.10 mmol, yield 91%). ^{1}H-NMR (400 MHz, DMSO-d_6, TMS): $\delta =$ 7.60–7.53 (m, 8H, Ar-CH), 7.25–7.18 (m, 8H, Ar-CH), 6.37 (s[br], Ar-NH + H_2O), 4.19 (q, 8H, CH_2), 2.81 (q, 2H, CH_2), 2.57 (q, 2H, CH_2). ^{13}C-NMR (400 MHz, DMSO-d_6, TMS): $\delta = 152.5$ (s, Ar-Cq), 136.5 (s, Ar-Cq), 122.5 (s, Ar-CH), 114.5 (s, Ar-CH), 66.6 (s, CH), 58.6 (s, CH_2), 51.9 (s, CH_2), MS (ESI; in MeOH): $m/z = [M+2Na]^{2+} = 393.23$, $[M+H]^+ = 611.30$, $[M+Na]^+ = 633.28$.

Synthesis of *N,N,N′,N′*-Tetrakis(2-(1-ethylbenzimidazolyl-methyl))-2-hydroxo-1,3-di-aminopropane (EtHPTB): In a 100 mL round-bottom flask 1.344 g fine-powdered NaOH (33.60 mmol) was suspended in 50 mL tetrahydrofuran. 4.885 g HPTB (8.000 mmol) was added and stirred for 30 h at room temperature to completely dissolve the ligand. Afterwards 10 mL bromoethane (14.6 g, 134 mmol) was added. The mixture was stirred for 48 h at room temperature. The milky suspension was evaporated to dryness and the faint yellow residue was extracted 3 times with 25 mL chloroform. The combined extracts were dried with sodium sulfate, filtrated and the filtrate was reduced to a minimal volume. The concentrated solution was added dropwise to 250 mL *n*-hexane under vigorous stirring to precipitate the product. The formed suspension was filtrated, the filter residue was under vacuum. The product was obtained as a colorless powder (5.343 g, 7.391 mmol, yield 92%). ^{1}H-NMR (400 MHz, $CDCl_3$, TMS): $\delta = 7.71$–7.64 (m, 4H, 4× Ar–CH), 7.25–7.16 (m, 12H, 12× Ar–CH), 5.06 (s[br], 1H, OH), 4.20 (m, 16H, 4×CH_2 + 4×CH_2), 3.77 (p, 1H, CH), 2.73 (dd, 4H, 2×CH_2), 1.11 (t, 12H, 4×CH_3). ^{13}C-NMR (400 MHz, $CDCl_3$, TMS): $\delta = 151.4$ (s, Ar–Cq), 142.3 (s, Ar–Cq), 134.7 (s, Ar–Cq), 122.6 (s, Ar–CH), 121.9 (s, Ar–CH), 119.5 (s, Ar–CH), 109.5 (s, Ar–CH), 68.9 (s, CH), 60.3 (s, CH_2), 52.0 (s, CH_2), 38.2 (s, CH_3). MS (ESI): $m/z = [M+2H]^{2+} = 362.22$, $[M+2Na]^{2+} = 393.17$; $[M+H]^+ = 723.43$; $[M+Na]^+ = 745.4060$.

Synthesis of $[Fe_2(EtHPTB)(OBz)](BPh_4)_2$ (1a): The synthesis was performed under inert conditions. 361 mg EtHPTB (0.50 mmol) and 50.5 mg Et_3N (0.50 mmol) were dissolved in 10 mL MeOH. A solution of 436 mg $Fe(OTf)_2 \times 2MeCN$ (1.00 mmol) in 3 mL MeOH was added to the ligand solution. After 5 min a solution of 61 mg and 50.5 mg Et_3N (0.50 mmol) was added dropwise to the complex solution. A precipitate was formed immediately. After 20 min the suspension was filtered and the filter residue was washed with MeOH and Et_2O. The crude product was dissolved in a minimal amount of acetone and stirred with 342 mg $NaBPh_4$ (1.00 mmol) overnight. After the solution was filtered, Et_2O was added until the solution became slightly cloudy. After two days at −30 °C light green crystals grew, which were suitable for single crystal X-ray diffraction analysis. The product was obtained as a slightly green powder (414 mg, 0.26 mmol, yield 51%). MS (ESI, 0.1% formic acid): $m/z = [Fe_2(EtHPTB)(OBz)(CHO_2H)]^+ = 1000.37$, $[Fe_2(EtHPTB)(CHO_2H)]^{2+} = 439.67$.

Synthesis of $[Fe_2(EtHPTB)(OH)_2(MeOH)_2](ClO_4)_3$ (1b): CAUTION! All perchlorate salts in this study should be handled with care because of their potential explosiveness. In a 250 mL round-bottom flask 2.184 g EtHPTB (3.000 mmol) were dissolved in 100 mL MeOH. A solution of 3.098 g $Fe(ClO_4)_3 \times 9\ H_2O$ (6.000 mmol) in 50 mL MeOH was added to this mixture. After 5 min 304 mg Et_3N (3.00 mmol) was added and stirred for 10 min. To the dark red solution another portion of 607 mg Et_3N (6.00 mmol) in 50 mL MeOH was added dropwise. The orange suspension was stirred for 30 min and then heated under reflux conditions for 30 min. After hot filtration of the solution the product was crystallized at room temperature. The crystals were filtered off and recrystallized twice in hot MeOH. The yellow crystals were filtered off and dried under vacuum. The obtained crystals were analyzed by single crystal X-ray diffraction. The product composition was determined by elemental analysis. The product was obtained as amber-colored powder (1.439 g, 1.170 mmol, yield 39%). MS (ESI; in MeOH): $m/z = [Fe_2(EtHPTB)(OMe)_3]^{2+} = 463.17$, $[Fe_2(EtHPTB)(OMe)_2(ClO_4)]^{2+} = 497.14$, $[Fe_2(EtHPTB)(OMe)_3(ClO_4)]^+ = 1025.29$. Elemental analysis calcd. (%) for $C_{45}H_{59}Cl_3Fe_2N_{10}O_{17}(+2H_2O)$: C(42.69), H(5.02), N(11.06). Found: C(42.50), H(4.85), N(11.19).

Synthesis of *N*-benzyl-*N,N′,N′*-tris(2-methylpyridyl)-ethylenediamine (bztpen): The synthesis was performed according to the procedure of Duelund *et al.*[23] In a 50 mL Schlenk-flask 751 mg *N*-benzylethylenediamine (5.00 mmol) and 2.63 g 2-Chloromethylpyridine hydrochloride (16.0 mmol) were dissolved in a mixture of 7.5 mL dichloromethane and 7.5 mL water. A solution of 1.28 g

NaOH (32 mmol) in 5 mL water was prepared. A third of this solution was added for the first 3 days. After the addition was complete, the solution was stirred for an additional 3 days at room temperature. The product was extracted 3 times with 10 mL dichloromethane. The combined organic phase was extracted with brine. The dichloromethane extract was dried over Na_2SO_4. The solvent was evaporated and the crude product was purified by column chromatography with silica as stationary phase (eluent: dichloromethane/MeOH). The product was obtained as a pale yellow solid (1.36 g, 3.21 mmol, yield 64%). ^{1}H-NMR (400 MHz, $CDCl_3$, TMS): $\delta = 8.52–8.44$ (m, 3H, 3×Ar–CH), 7.60–7.53 (m, 3H, 3×Ar–CH), 7.49–7.39 (m, 3H, 3×Ar–CH), 7.32–7.17 (m, 5H, 5×Ar–CH), 7.14–7.07 (m, 3H, 3×Ar–CH), 3.78 (s, 4H, 2×CH_2), 3.72 (s, 2H, –CH_2), 3.59 (s, 2H, –CH_2), 2.82–2.62 (m, 4H, 2×CH_2). ^{13}C-NMR (400 MHz, $CDCl_3$, TMS): $\delta = 150.0$ (s, Ar–CH), 148.9 (s, Ar–Cq), 136.3 (s, Ar–CH), 128.8 (s, Ar–Cq), 128.2 (s, Ar–CH), 126.9 (s, Ar–Cq), 122.8 (s, Ar–CH), 121.8 (s, Ar–CH), 121.6 (s, Ar–CH), 60.8 (s, 2×CH_2), 60.6 (s, –CH_2), 59.0 (s, –CH_2), 52.2 (s, –CH_2), 51.4 (s, –CH_2). MS (ESI): $m/z = [M+H]^+ = 424.25$.

Synthesis of [Fe(bztpen)(OMe)](ClO$_4$)$_2$ (3): CAUTION! All perchlorate salts in this study should be handled with care because of their potential explosiveness. In a 25 mL round-bottom flask 847 mg bztpen (2.00 mmol) were dissolved in 15 mL MeOH. A solution of 1.03 g $Fe(ClO_4)_3 \times 9H_2O$ (2.00 mmol) in 5 mL MeOH was added dropwise to this mixture. With vigorous stirring, the solution was triturated with 291 µL Et_3N (2.10 mmol). After 15 min the product was precipitated by adding Et_2O to the yellow solution. The crude product was recrystallized in hot MeOH. The yellow crystals were filtered off and dried under vacuum. The obtained crystals were suitable for single crystal X-ray diffraction. The product was obtained as yellow powder (1.10 g, 1.36 mmol, yield 68%). MS (ESI): $m/z = [M+MeO]^+ = 541.22$. Elemental analysis calcd. (%) for $C_{28}H_{32}Cl_2FeN_5O_9(+H_2O)$: C(46.24), H(4.71), N(9.63). Found: C(46.22), H(4.40), N(9.54).

Synthesis of perdecanoic acid (PDA): Synthesized according to literature.[15] In a 250 mL round-bottom flask 10.0 g decanoic acid (58.1 mmol) were dissolved in 20 mL conc. sulfuric acid ($\omega = 98\%$). The mixture was cooled in an ice bath to keep the temperature around 10 °C. Under stirring and proceeded cooling 5 mL of a H_2O_2 solution ($\omega = 50\%$) was added dropwise over the course of 20 min. The temperature should not rise above 20 °C during the addition. After the addition, the mixture was allowed to stir for another 50 min at 10 °C. The reaction mixture was then slowly diluted with 75 mL ice-cold water, in which the temperature should not rise above 30 °C. The product was extracted five times with 15 mL Et_2O using a separatory funnel. The combined organic phase was extracted twice with 15 mL water. The organic phase was dried over Na_2SO_4 and the filtrate was removed on a rotary evaporator at 25 °C (CAUTION!). The colorless residue was dissolved in 100 mL *n*-hexane and crystallized at −30 °C overnight. The crystals were filtered off and rinsed with cold *n*-hexane. The product was carefully dried under vacuum. The product was obtained as colorless crystals (6.77 g, 36.0 mmol, yield 62%). ^{1}H-NMR (400 MHz, $CDCl_3$, TMS): $\delta = 11.49$ (s[br], 1H, –CO_3H), 2.42 (t, 2H, –CH_2), 1.70 (quint, 2H, –CH_2), 1.40–1.19 (m, 12H, 6×CH_2), 0.88 (t, 3H, –CH_3). ^{13}C-NMR (400 MHz, $CDCl_3$, TMS): $\delta = 174.7$ (s, Cq), 31.8 (s, –CH_2), 30.4 (s, –CH_2), 29.3 (s, –CH_2), 29.2 (s, –CH_2), 29.1 (s, –CH_2), 28.9 (s, –CH_2), 24.6 (s, –CH_2), 22.7 (s, –CH_2), 14.1 (s, –CH_3). MS (ESI): $m/z = [M+H]^+ = 189.15$, $[M+Na]^+ = 211.13$.

Deposition Numbers 2088347 (for **3**), 2088348 (for **1b**$(ClO_4)_3$), 2088349 (for **1a**$(BPh_4)_2$), and 2101789 (for PDA) contain the supplementary crystallographic data for this paper. These data are provided free of charge by the joint Cambridge Crystallographic Data Centre and Fachinformationszentrum Karlsruhe Access Structures service www.ccdc.cam.ac.uk/structures.

Acknowledgements

We gratefully acknowledge support by the Justus-Liebig-Universität Gießen. A.J.A. and D.M. wish to express thanks for the support by the administrators of the JustHPC-cluster of the Justus-Liebig-Universität, Gießen. Open Access funding enabled and organized by Projekt DEAL.

Conflict of Interest

The authors declare no conflict of interest.

Keywords: Iron · Kinetics · Reaction mechanisms · Substituent effects · Time-resolved spectroscopy

[1] a) J. Piera, J.-E. Bäckvall, *Angew. Chem. Int. Ed.* **2008**, *47*, 3506–352; *Angew. Chem.* **2008**, *120*, 3558–35763; b) J. Dong, E. Fernández-Fueyo, F. Hollmann, C. E. Paul, M. Pesic, S. Schmidt, Y. Wang, S. Younes, W. Zhang, *Angew. Chem. Int. Ed.* **2018**, *57*, 9238–926; *Angew. Chem.* **2018**, *130*, 9380–94041.
[2] A. L. Feig, S. J. Lippard, *J. Am. Chem. Soc.* **1994**, *116*, 8410–8411.
[3] U. K. Bagha, J. K. Satpathy, G. Mukherjee, C. V. Sastri, S. P. de Visser, *Org. Biomol. Chem.* **2021**, *19*, 1879–1899.
[4] B. Kripli, F. V. Csendes, P. Török, G. Speier, J. Kaizer, *Chem. Eur. J.* **2019**, *25*, 14290–14294.
[5] a) Y. Dong, S. Yan, V. G. Young Jr., L. Que Jr., *Angew. Chem. Int. Ed.* **1996**, *35*, 618–620; *Angew. Chem.* **1996**, *108*, 673–676; b) L. Westerheide, F. K. Müller, R. Than, B. Krebs, J. Dietrich, S. Schindler, *Inorg. Chem.* **2001**, *40*, 1951–1961; c) A. L. Feig, M. Becker, S. Schindler, R. van Eldik, S. J. Lippard, *Inorg. Chem.* **1996**, *35*, 2590–2601; d) Y. Dong, S. Menage, B. A. Brennan, T. E. Elgren, H. G. Jang, L. L. Pearce, L. Que Jr., *J. Am. Chem. Soc.* **1993**, *115*, 1851–1859.
[6] A. Miska, D. Schurr, G. Rinke, R. Dittmeyer, S. Schindler, *Chem. Eng. Sci.* **2018**, *190*, 459–465.
[7] a) I. Bernal, I. M. Jensen, K. B. Jensen, C. J. McKenzie, H. Toftlund, J.-P. Tuchagues, *J. Chem. Soc. Dalton Trans.* **1995**, 3667–3675; b) A. Hazell, C. J. McKenzie, L. P. Nielsen, S. Schindler, M. Weitzer, *J. Chem. Soc. Dalton Trans.* **2002**, 310; c) T. Nebe, A. Beitat, C. Würtele, C. Dücker-Benfer, R. van Eldik, C. J. McKenzie, S. Schindler, *Dalton Trans.* **2010**, *39*, 7768–7773.
[8] F. Avenier, C. Herrero, W. Leibl, A. Desbois, R. Guillot, J.-P. Mahy, A. Aukauloo, *Angew. Chem. Int. Ed.* **2013**, *52*, 3634–3637; *Angew. Chem.* **2013**, *125*, 3722–3725.
[9] a) R. Than, A. Schrodt, L. Westerheide, R. van Eldik, B. Krebs, *Eur. J. Inorg. Chem.* **1999**, *1999*, 1537–1543; b) B. A. Brennan, Q. Chen, C. Juarez-Garcia, A. E. True, C. J. O'Connor, L. Que, *Inorg. Chem.* **1991**, *30*, 1937–1943;
[10] H. H. Awad, D. M. Stanbury, *Int. J. Chem. Kinet.* **1993**, *25*, 375–381.
[11] D. A. Wink, J. F. Darbyshire, R. W. Nims, J. E. Saavedra, P. C. Ford, *Chem. Res. Toxicol.* **1993**, *6*, 23–27.
[12] W. C. Nottingham, J. R. Sutter, *Int. J. Chem. Kinet.* **1986**, *18*, 1289–1302.
[13] U. Pinkernell, H.-J. Lüke, U. Karst, *Analyst* **1997**, *122*, 567–571.
[14] S. Hochreuther, S. T. Nandibewoor, R. Puchta, R. van Eldik, *Dalton Trans.* **2012**, *41*, 512–522.
[15] M. Sitko, A. Szelwicka, A. Wojewódka, A. Skwarek, D. Tadasiewicz, L. Schimmelpfennig, K. Dziuba, M. Morawiec-Witczak, A. Chrobok, *RSC Adv.* **2019**, *9*, 30012–30018.
[16] a) A. M. Zima, O. Y. Lyakin, R. V. Ottenbacher, K. P. Bryliakov, E. P. Talsi, *ACS Catal.* **2017**, *7*, 60–69; b) J. Serrano-Plana, W. N. Oloo, L. Acosta-Rueda, K. K. Meier, B. Verdejo, E. Garcia-Espana, M. G. Basallote, E. Münck, L. Que Jr., A. Company, M. Costas, *J. Am. Chem. Soc.* **2015**, *137*, 15833–15842; c) Y. Wang, D. Janardanan, D. Usharani, K. Han, L. Que Jr., S. Shaik, *ACS Catal.* **2013**, *3*, 1334–1341; d) C. Wegeberg, W. R. Browne, C. J. McKenzie, *ACS Catal.* **2018**, *8*, 9980–9991; e) J. Serrano-Plana, F. Acuña-Parés, V. Dantignana, W. N. Oloo, E. Castillo, A. Draksharapu, C. J. Whiteoak, V. Martin-Diaconescu, M. G. Basallote, J. M. Luis, L. Que, M. Costas, A. Company, *Chem. Eur. J.* **2018**, *24*, 5331–5340; f) S. Kal, S. Xu, L.

Que Jr., *Angew. Chem. Int. Ed.* **2020**, *59*, 7332–7349; *Angew. Chem.* **2020**, *132*, 7400–7419; g) R. Fan, J. Serrano-Plana, W. N. Oloo, A. Draksharapu, E. Delgado-Pinar, A. Company, V. Martin-Diaconescu, M. Borrell, J. Lloret-Fillol, E. Garcia-Espana, Y. Guo, E. L. Bominaar, L. Que Jr., M. Costas, E. Münck, *J. Am. Chem. Soc.* **2018**, *140*, 3916–3928; h) J. Serrano-Plana, A. Aguinaco, R. Belda, E. García-España, M. G. Basallote, A. Company, M. Costas, *Angew. Chem. Int. Ed.* **2016**, *55*, 6310–6314; *Angew. Chem.* **2016**, *128*, 6418–6422; i) W. N. Oloo, R. Banerjee, J. D. Lipscomb, L. Que Jr., *J. Am. Chem. Soc.* **2017**, *139*, 17313–17326.

[17] X. Zhang, H. Furutachi, T. Tojo, T. Tsugawa, S. Fujinami, T. Sakurai, M. Suzuki, *Chem. Lett.* **2011**, *40*, 515–517.

[18] N. A. Ortega-Villar, M. C. Munoz, J. A. Real, *Eur. J. Inorg. Chem.* **2010**, *2010*, 5563–5567.

[19] J. R. Khusnutdinova, J. Luo, N. P. Rath, L. M. Mirica, *Inorg. Chem.* **2013**, *52*, 3920–3932.

[20] A. Zhou, S. T. Kleespies, K. M. van Heuvelen, L. Que Jr., *Chem. Commun.* **2015**, *51*, 14326–14329.

[21] H. Miyamoto, Y. Yampolski, C. L. Young, *J. Phys. Chem. Ref. Data.* **2014**, *43*, 33102.

[22] V. McKee, M. Zvagulis, J. V. Dagdigian, M. G. Patch, C. A. Reed, *J. Am. Chem. Soc.* **1984**, *106*, 4765–4772.

[23] L. Duelund, R. Hazell, C. J. McKenzie, L. Preuss Nielsen, H. Toftlund, *J. Chem. Soc. Dalton Trans.* **2001**, 152–156.

[24] a) S. Grimme, S. Ehrlich, L. Goerigk, *J. Comput. Chem.* **2011**, *32*, 1456–1465; b) S. Grimme, J. Antony, S. Ehrlich, H. Krieg, *J. Chem. Phys.* **2010**, *132*, 154104; c) M. Reiher, O. Salomon, B. Artur Hess, *Theor. Chem. Acc.* **2001**, *107*, 48–55; d) F. Weigend, M. Häser, H. Patzelt, R. Ahlrichs, *Chem. Phys. Lett.* **1998**, *294*, 143–152; e) F. Weigend, R. Ahlrichs, *Phys. Chem. Chem. Phys.* **2005**, *7*, 3297–3305; f) K. Eichkorn, F. Weigend, O. Treutler, R. Ahlrichs, *Theor. Chem. Acc.* **1997**, *97*, 119–124; g) S. H. Vosko, L. Wilk, M. Nusair, *Can. J. Phys.* **1980**, *58*, 1200–1211; h) J. C. Slater, *Phys. Rev.* **1951**, *81*, 385–390; i) *Proc. R. Soc. Lond. A* **1929**, *123*, 714–733; j) A. D. Becke, *J. Chem. Phys.* **1993**, *98*, 5648–5652; k) Lee, Yang, Parr, *Phys. Rev. B Condens Matter* **1988**, *37*, 785–789; l) Becke, *Phys. Rev. A Gen. Phys.* **1988**, *38*, 3098–3100.

[25] a) A. Klamt, G. Schüürmann, *J. Chem. Soc. Perkin Trans. 2* **1993**, 799–805; b) A. Schäfer, A. Klamt, D. Sattel, J. C. W. Lohrenz, F. Eckert, *Phys. Chem. Chem. Phys.* **2000**, *2*, 2187–2193;

[26] a) S. G. Balasubramani, G. P. Chen, S. Coriani, M. Diedenhofen, M. S. Frank, Y. J. Franzke, F. Furche, R. Grotjahn, M. E. Harding, C. Hättig, A. Hellweg, B. Helmich-Paris, C. Holzer, U. Huniar, M. Kaupp, A. Marefat Khah, S. Karbalaei Khani, T. Müller, F. Mack, B. D. Nguyen, S. M. Parker, E. Perlt, D. Rappoport, K. Reiter, S. Roy, M. Rückert, G. Schmitz, M. Sierka, E. Tapavicza, D. P. Tew, C. van Wüllen, V. K. Voora, F. Weigend, A. Wodyński, J. M. Yu, *J. Chem. Phys.* **2020**, *152*, 184107; b) TURBOMOLE V7.5 2020, a development of University of Karlsruhe and Forschungszentrum Karlsruhe GmbH, 1989–2007, *TURBOMOLE GmbH*, since **2007**; available from *https://www.turbomole.org*.

[27] a) M. Reiher, *Inorg. Chem.* **2002**, *41*, 6928–6935; b) K. P. Kepp, *Inorg. Chem.* **2016**, *55*, 2717–2727; c) O. Salomon, M. Reiher, B. A. Hess, *J. Chem. Phys.* **2002**, *117*, 4729–4737.

[28] a) Perdew, Burke, Ernzerhof, *Phys. Rev. Lett.* **1996**, *77*, 3865–3868; b) Perdew, Wang, *Phys. Rev. B Condens.Matter* .**1992**, *45*, 13244–13249; c) J. P. Perdew, M. Ernzerhof, K. Burke, *J. Chem. Phys.* **1996**, *105*, 9982–9985; d) A. Schäfer, H. Horn, R. Ahlrichs, *J. Chem. Phys.* **1992**, *97*, 2571–2577.

[29] a) R. Ahlrichs, M. Bär, M. Häser, H. Horn, C. Kölmel, *Chem. Phys. Lett.* **1989**, *162*, 165–169; b) P. Deglmann, F. Furche, *J. Chem. Phys.* **2002**, *117*, 9535–9538; c) P. Deglmann, F. Furche, R. Ahlrichs, *Chem. Phys. Lett.* **2002**, *362*, 511–518; d) TURBOMOLE V7.3 2018, a development of University of Karlsruhe and Forschungszentrum Karlsruhe GmbH, 1989–2007, *TURBOMOLE GmbH*, since **2007**; available from *http://www.turbomole.com*.

Manuscript received: August 16, 2021
Revised manuscript received: September 10, 2021
Accepted manuscript online: September 14, 2021